THE JOURNAL OF BIOLOGICAL CHEMISTRY
Vol. 278, No. 40, Issue of October 3, pp. 38892–38901, 2003

Printed in U.S.A.

The Apical Loop of the HIV-1 TAR RNA Hairpin Is Stabilized by a Cross-loop Base Pair*

Received for publication, February 24, 2003, and in revised form, July 24, 2003
Published, JBC Papers in Press, July 25, 2003, DOI 10.1074/jbc.M301939200

Tadeusz Kulinski‡§, Mikolaj Olejniczak‡, Hendrik Huthoff§¶, Lukasz Bielecki‡, Katarzyna Pachulska-Wieczorek‡, Atze T. Das¶, Ben Berkhout¶, and Ryszard W. Adamiak‡‖

From the ‡Institute of Bioorganic Chemistry, Polish Academy of Sciences, Noskowskiego 12-14, 61-704 Poznañ, Poland and the ¶Department of Human Retrovirology, Academic Medical Center, University of Amsterdam, 1105AZ Amsterdam, The Netherlands

The TAR hairpin of the HIV-1 RNA genome is indispensable for trans-activation of the viral promoter and virus replication. The TAR structure has been studied extensively, but most attention has been directed at the three-nucleotide bulge that constitutes the binding site of the viral Tat protein. In contrast, the conformational properties of the apical loop have remained elusive. We performed biochemical studies and molecular dynamics simulations, which indicate that the TAR loop is structured and stabilized by a cross-loop base pair between residues C^{30} and G^{34}. Mutational disruption of the cross-loop base pair results in reduced Tat response of the LTR promoter, which can be rescued by compensatory mutations that restore the base pair. Thus, Tat-mediated transcriptional activation depends on the structure of the TAR apical loop. The C^{30}–G^{34} cross-loop base pair classes TAR in a growing family of hairpins with a structured loop that was recently identified in ribosomal RNA, tRNA, and several viral and cellular mRNAs.

The HIV-1[1] life cycle depends on specific RNA-protein interactions. The 5′-end of all HIV-1 transcripts contains a 59-nucleotide stem-loop structure termed the trans-activation response element (TAR). Understanding of the TAR RNA structure, its dynamics and interaction with proteins is of importance for the design of potential therapeutic antiviral strategies (1). TAR RNA is indispensable for HIV-1 transcriptional regulation of the long-terminal repeat (LTR) promoter. Sp1 driven basal transcription at the LTR allows the production of a low level of HIV-1 transcripts needed for the synthesis of the viral transactivator protein, Tat (2–4). The TAR hairpin serves as a binding site for Tat and the interaction between the protein and RNA strongly stimulates the activity of the LTR promoter (5–11). Several cellular proteins that stimulate the expression of TAR-containing transcripts have been identified (12–21). Currently, the best studied cellular component of the Tat-activated phase of LTR transcription is the positive transcriptional elongation factor (pTEFb). The pTEFb complex associates with TAR through its cyclin T1 subunit in a Tat-dependent manner. Binding of Tat to a three-nucleotide bulge in TAR facilitates the interaction of cyclin T1 with the TAR apical loop (13, 22, 23). The kinase component of P-TEFb, CDK9, can then phosphorylate the C-terminal domain of RNA polymerase II, which enhances the processivity of the elongating polymerase (24–26).

The binding of Tat to the TAR bulge has been studied extensively. Numerous studies have addressed the structure of both the free TAR RNA (27–29) and TAR bound to substrates such as argininamide (27), Tat-related peptides (29, 30), small inhibitor molecules (31) and cations (32, 33). In addition, molecular dynamics simulations of TAR have been reported (34, 35). From these studies it is apparent that the conformation of the bulge differs significantly in the absence and presence of the Tat protein. The bulge residues are partially stacked in the free TAR RNA. Upon binding of Tat, the bulge is extruded from the TAR helix and a base triple is formed that involves the first bulge residue U^{23} and the A^{27}–U^{38} base pair. The binding of Tat to TAR thus coincides with a dramatic change in the tertiary structure of TAR, which may occur by an induced fit or conformational capture mechanism (36).

In contrast, little is known about the structural properties of the six-nucleotide apical loop of the TAR hairpin. NMR studies demonstrated considerable conformational flexibility in the loop with a tendency to form a compact loop structure (30, 37, 38). It appears that the most structured regions are at either end of the loop, consistent with stacking of loop residues on the stem-closing base pair (30, 37, 39). Analysis of chemical shifts observed for ^{13}C-adenosine enriched TAR residues (38) and relaxation experiments suggested that A^{35} has an unusual local environment and is extruded from the apical loop (40). A few investigators have proposed distinct structural features of the apical TAR loop. The possibility of a protonated non-canonical C^{30}–$A^{35}H^{+}$ base pair, yielding a tetraloop structure for TAR has been suggested (39). Alternatively, a cross-loop base pair involving residue C^{30} and the penultimate loop residue G^{34} has been proposed (41). This interaction has been observed transiently in molecular dynamics simulations (34, 35), and it was recently suggested that the C^{30}–G^{34} cross-loop base pair is required for binding of cyclin T1 (42).

In this study, we specifically address the structure of the TAR loop and its involvement in the HIV-1 LTR promoter activity. We present evidence that the TAR apical loop can indeed form the C^{30}–G^{34} base pair. Biochemical studies and

* This work was supported by grants from the State Committee for Scientific Research, Republic of Poland (8T11F00219, 7T09A09720) and the Netherlands Organization for Scientific Research (NWO-CW). The costs of publication of this article were defrayed in part by the payment of page charges. This article must therefore be hereby marked "*advertisement*" in accordance with 18 U.S.C. Section 1734 solely to indicate this fact.

This article is dedicated to Professor Maciej Wiewiórowski on the occasion of his 85th birthday anniversary.

§ These authors contributed equally to this work.

‖ To whom correspondence should be addressed: Institute of Bioorganic Chemistry, Polish Academy of Sciences, Noskowskiego 12-14, 61-704 Poznañ, Poland. Tel.: 48-61-8528503; Fax: 48-61-8520532; E-mail: adamiakr@ibch.poznan.pl.

[1] The abbreviations used are: HIV-1, human immunodeficiency virus type 1; TAR, transactivator response element; Tat, trans-activator of HIV gene expression; AP, 2-aminopurine; MD, molecular dynamics; DMS, dimethylsulfate; LTR, long terminal repeat; RMSD, root mean-squared deviation; nt, nucleotides.

molecular dynamics with a model TAR hairpin, and modified analogues thereof, indicate that residue G^{34} is oriented inside the loop. G^{34} can form relatively stable hydrogen bonds with C^{30}. The C^{30}–G^{34} base pair stacks on the C^{29}–G^{36} closing base pair of the stem. Subsequent analysis of mutant TAR constructs in LTR-luciferase assays confirmed the importance of the cross-loop base pair in Tat-mediated transcriptional activation.

EXPERIMENTAL PROCEDURES

Oligoribonucleotide Synthesis—The synthesis of 29-mer HIV-1 TAR RNA and its 2-aminopurine riboside modified analogues AP34 and AP35 was performed using solid-support aided phoshoramidite chemistry and applying the 2′-*O*-tBDMSi protection (43). After 1 μmol of scale synthesis and deprotection with fluoride ion, the RNA was purified by preparative 19% polyacrylamide gel electrophoresis under denaturing conditions, followed by electroelution with a Biotrap BT 1000 and desalting on NAP columns. The sequence of the oligomers was confirmed by RNA sequencing with ribonuclease T1.

UV Melting and Thermodynamics—UV melting of the chemically synthesized oligomers was measured on a temperature controlled Beckman DU70 spectrophotometer in the temperature range from 10 to 98 °C (heating rate of 1.0 °C min^{-1}, sampling at each 0.3 °C). The buffer for thermodynamic studies was 1 M NaCl, 10 mM phosphate (pH 7.0). The RNA concentrations, varied over 50-fold range, were calculated from the absorbance at 260 nm measured at 80 °C using single-strand extinction coefficients approximated by a nearest-neighbor model. Unimolecular hairpin formation was checked by oligomer concentration dependence of the UV melting profiles. Prior to the measurement, the RNA was renatured by incubation at 85 °C for 3 min, followed by slow cooling to room temperature. Absorbance *versus* temperature profiles were fit to two-state transition model with sloping baselines by using the nonlinear least-squares program MeltWin. The experiments were repeated 3–5 times.

Thermal denaturation of *in vitro* synthesized 1/466 HIV-1 RNA was measured on a PerkinElmer Life Sciences Lambda 2 spectrophotometer at a heating rate of 0.5 °C min^{-1} with sampling at each 0.1 °C. Samples contained ~3.0 μg of RNA dissolved in 140 μl of 50 mM sodium Cacodylate buffer (pH 7.2). Prior to the measurement, the RNA was renatured by incubation at 37 °C for 30 min. Electrophoretic analysis of the samples prior to the analysis confirmed the monomeric state of the RNA. No significant degradation of the transcripts was apparent after the measurement as judged by analysis of the RNA on a sequencing gel.

Pb^{2+}-induced RNA Phosphodiester Bond Cleavage—The oligoribonucleotides were 5′-end-labeled using T4 polynucleotide kinase, gel purified and quantitated on a Beckmann LS5000TA scintillation counter. The RNA was refolded by heating at 80 °C for 30 s, followed by slow cooling to room temperature in a buffer containing 10 mM Tris-HCl, pH 7.2, 40 mM NaCl, 10 mM $MgCl_2$, and 8 μM carrier tRNA. Freshly prepared $Pb(OAc)_2$ was added to final concentrations of 0.5, 1, and 2 mM. This reaction mixture was incubated for 15 min at room temperature. At least three independent experiments were performed with each oligomer.

RNA cleavage ladders were generated by boiling the RNA in formamide for 40 min. G-specific sequencing ladders were generated by incubation with 0.2 units/μl RNase T1 in 50 mM sodium citrate (pH 4.5) and 7 M urea for 10 min at 55 °C. All reactions were quenched by the addition of the equal volume of gel loading buffer (8 M urea, 20 mM EDTA, tracking dyes) and transferred to dry ice. Reaction products were separated by 19% PAGE (8 M urea). Cleavages were visualized and quantitatively analyzed using a Typhoon 8600 apparatus with ImageQuant software. The images were not edited and linear relationship between signal and image intensity was retained.

Modeling and Molecular Dynamics Simulations—The 29-mer RNA models of the wild-type sequence and mutants AP34 and AP35 were built using the Amber 4.1 (44) suite of programs and the initial coordinates according to model #17 of TAR from the 1ANR PDB file (30). The force field parameters for 2-aminopurine riboside were developed using the Gaussian 94 (45) and Resp (46) programs. Na^+ counterions were added and solvated in a rectangular periodic boundary conditions box, an 8.5 Å thick water layer was maintained in all dimensions around the RNA molecules. The simulations were carried out with the Sander module using the Amber force field (44) on a Cray J916 computer. The protocol for the simulations consisted of an equilibration procedure followed by up to 1.6 ns of unrestrained molecular dynamics in 300 K with the long-range electrostatic interactions treated using the particle-mesh Ewald summation method (PME) (47). Frames were collected every 1 ps. Conformational analysis was based on the last 50 non-minimized frames.

Models of the 14-mer TAR RNA mini-hairpin (fragment 26–39) were built using the INSIGHTII program. Coordinates for the backbone of an initial structure were taken from the NMR structure of the adenosine-rich hexaloop RNA hairpin (PDB code 1bvj) (48). The HIV-1 TAR sequence was modeled onto the structure by appropriate base substitutions, while keeping the original orientation of the replaced bases. The structure was subsequently minimized and remodeled. The resulting models of the hairpin were solvated in a water box containing TIP3P water. 13 Na^+ ions were added to neutralize system. The whole system was first minimized with harmonic constraints applied to the RNA and finally, without any constraints. Molecular dynamics simulations were performed using the CHARMM version 27 program, and force field parameters Charmm27 (49) on a Pentium III multiprocessor cluster. MD simulations of each model started with heating the whole system from 50 to 300 K, 320 K, or 340 K in 6 ps followed by 4 ps of equilibration. MD simulations where run in the NVE ensemble, using periodic boundary condition, time step 0.002 ps and the SHAKE algorithm. Frames were collected every 2 ps. The trajectories collected at given temperatures were searched for the regions showing low RMSD, displaying locally stable conformations of the apical loop structure.

In Vitro Transcription—PCR products to be used as DNA templates for *in vitro* transcription were generated as described previously (50). To produce transcript in which the sequence of the TAR loop (GGG, nt 32–34) was changed to AAA, the PCR was performed with an antisense primer termed TAR T7 AAA: (5′-AAT TCT AAT ACG ACT CAC TAT AGG GTC TCT CTG GTT AGA CCA GAT TTG AGC CUA AAA GCT CTC TGG-3′). The 466-nt HIV-1 transcripts were synthesized from PCR templates with the Ambion T7 megashortscript transcription kit following the manufacturer's instructions. The RNA was excised from a 4% denaturing polyacrylamide gel, using UV shadowing for visualization. The RNA was eluted from the gel slice by overnight incubation in 1× Tris/borate EDTA buffer at 4 °C and continuous shaking. After precipitation and ethanol washing the RNA was dissolved in demineralized water, heated at 80 °C and cooled slowly to room temperature. Aliquots were stored at −20 °C.

RNA Structure Probing—For chemical structure probing, 2 μg of *in vitro* synthesized RNA corresponding to the first 80 nucleotides of HIV-1 transcripts (1–80) was dissolved in water and heated to 80 °C. Tubes were then placed in a 60 °C water bath, salt was added and the solution was allowed to slowly cool to 37 °C. Final solutions contained 50 mM Na Cacodylate buffer (pH 7.2) and 1.0 mM $MgCl_2$ in a total volume of 100 μl. A volume of 1.0 μl of DMS or kethoxal was added and allowed to react for 5 and 15 min, respectively. Reactions were stopped by adding 5 μl of 10 μg/μl total *Escherichia coli* tRNA and subsequent precipitation with ammonium acetate. The precipitated RNA was dissolved in 10 μl of water, of which 2 μl was used for primer extension reactions. The primer used anneals to nucleotides 61–80 of the transcript, primer R80/61. Reverse transcription with the AMV reverse transcriptase was performed as described previously (50). Samples were precipitated and loaded on a 10% denaturing polyacrylamide gel. The intensity of reverse transcriptase stops caused by base modification was analyzed on a Storm 860 phosphorimager.

Plasmid Constructs—The pBlue3′LTR-luc plasmid contains an *Xho*I-*Hin*dIII fragment from the HIV-1 LAI proviral DNA, encoding the complete U3 region, the transcription start site (+1) and R sequences up to position +82, coupled to the Firefly luciferase reporter gene (51). For mutation of the TAR hairpin, a PCR was performed with the primer LAI5′X (5′-CAT TCT AGA TGG AAG GGC TAA TTC ACT CCC-3′) and one of the following a mutagenic primers (substituted nucleotides underlined): TAR(U30G34): 5′-AGG CTT AAG CAG TGG GTT CCC TAG TTA GCC AGA GAG CTC CCA AGC TCA A-3′; TAR(C30A34) 5′-GAG GCT TAA GCA GTG GGT TCC CTA GTT AGC CAG AGA GCT TCC AGG-3′; TAR(U30A34) 5′-GAG GCT TAA GCA GTG GGT TCC CTA GTT AGC CAG AGA GCT TCC AAG CTC AA-3′; TAR(G30G34): 5′-AGG CTT AAG CAG TGG GTT CCC TAG TTA GCC AGA GAG CTC CCA CGC TCA A-3′; TAR(C30C34) 5′-GAG GCT TAA GCA GTG GGT TCC CTA GTT AGC CAG AGA GCT GCC AGG-3′; TAR(G30C34) 5′-GAG GCT TAA GCA GTG GGT TCC CTA GTT AGC CAG AGA GCT GCC ACG CTC AA-3′. The PCR fragments were digested with *Bfr*I and *Dra*III and cloned in the corresponding sites of pBlue3′LTR-luc. All mutations were verified by sequence analysis. The pRL-CMV plasmid contains the *Renilla* luciferase reporter gene and the CMV promoter elements and is used as an internal control reporter plasmid in transfection assays. pcDNA3-Tat expresses the HIV-1 LAI Tat gene under control of the CMV promoter (52).

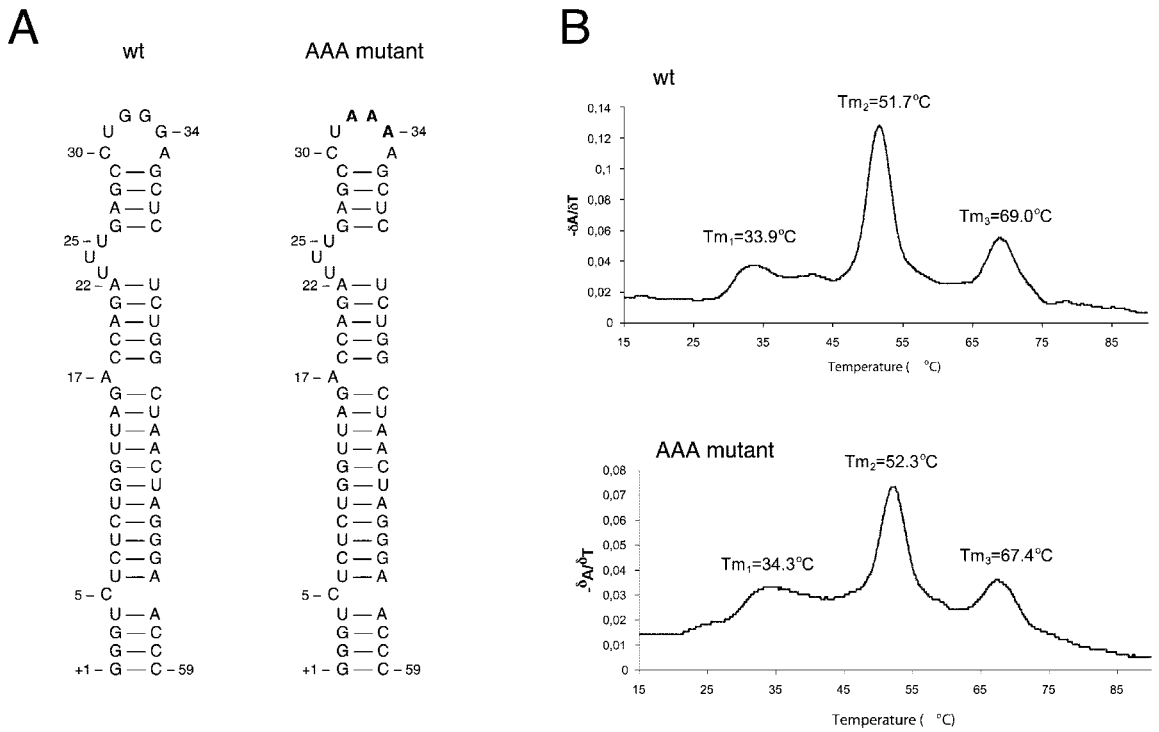

FIG. 1. **Thermal denaturation of 466 nt HIV-1 transcripts with the wild-type or AAA mutant TAR sequence.** *A*, secondary structure models of the wild-type and mutant TAR elements. *Bold letters* indicate mutant residues in the TAR apical loop. *B,* thermal denaturation profiles of the wild-type and AAA mutant HIV-1 RNA, shown as the first order derivative. The T_m of the various melting points is indicated above the corresponding transition. Spectra were recorded at 260 nm in 50 mM sodium cacodylate buffer with pH 7.

Cells and Transfection—Transfection of C33A was performed the calcium phosphate method as previously described (53). SupT1 T cells were grown in RPMI 1640 medium containing 10% fetal calf serum at 37 °C and 5% CO_2. Cells were transfected by electroporation. 5×10^6 cells were washed in RPMI 1640 with 20% fetal calf serum, mixed with DNA in 0.4-cm cuvettes and electroporated at 250 volts and 960 μF, and then resuspended in RPMI 1640 with 10% fetal calf serum. The transcriptional activity of the wild-type and TAR-mutated HIV-1 LTRs was determined by transfection of SupT1 T cells with 5 μg of wild-type or TAR mutated pBlue3′LTR-luc, 0.5 μg of pRL-CMV, with or without 0.5 μg of pcDNA3-Tat. At 2 days after transfection, cells were isolated by centrifugation at 260 g for 10 min. The Dual-Luciferase Reporter assay system was used to determine the firefly and *Renilla* luciferase levels.

Comparative Sequence Analysis—Sequences of different HIV-1 isolates were obtained from the HIV data base at Los Alamos (//-web.lanl.gov/). Only isolates with a complete TAR sequence were considered in the analysis, yielding a total of 654 sequences from most of the prevailing HIV-1 subtypes.

RESULTS

Thermal Denaturation of HIV-1 RNA with a Mutated TAR Loop—To test if the TAR loop is structured, we performed a UV-melting experiment with transcripts corresponding to the 5′-terminal 466 nucleotides of the wild-type HIV-1 RNA and a mutant in which the apical loop residues 32–34 were changed from GGG to AAA (Fig. 1). Three discrete transitions are apparent for both transcripts, which we termed T_{m1}, T_{m2}, and T_{m3}. The high-temperature transition T_{m3} has previously been shown to correspond to the TAR hairpin, and the intense T_{m2} transition reflects melting of the extended LDI stem in the downstream leader domain (50). T_{m1} is a rather diffuse transition that occurs at low temperature, which may suggest melting of a tertiary structure motif in the HIV-1 RNA. The melting temperatures of T_{m1} and T_{m2} are similar for the wild-type RNA and the AAA mutant, but we consistently observed a difference of 1.6 °C for the TAR melting transition T_{m3}. This difference is significantly higher than the experimental variation that we measured for duplicate samples (<0.5 °C). Thus, the sequence change in the loop has destabilized the TAR hairpin, which indicates that the loop is structured and contributes to the stability of the TAR hairpin.

Electrophoretic and Thermodynamic Properties of 2-Aminopurine-substituted TAR Hairpins—To study the structure of the TAR loop in more detail, we synthesized 29-mer TAR hairpins with the wild-type sequence and 2-aminopurine substitutions at position 34 or 35 (Fig. 2*A*). When these oligoribonucleotides were checked for their purity in denaturing PAGE, all three fragments demonstrated the same electrophoretic mobility (results not shown). However, under non-denaturing PAGE conditions, the modified hairpin AP34 exhibits significantly increased mobility compared with the wild-type hairpin (Fig. 2*B*). In contrast, the AP35 hairpin shows practically the same mobility as the wild-type hairpin. This effect was independent of different incubation procedures used for refolding of the RNA prior to non-denaturing PAGE (results not shown). Thus, the different electrophoretic mobility of hairpin AP34 indicates a substantial change in the structural properties of its apical loop in comparison with the wild-type and AP35 hairpins.

Next, we performed melting experiments with the 29-mer hairpins and derived the thermodynamic parameters by numerical analysis (Table I). Each hairpin melts in a single transition and melting temperatures (T_m) were independent on the RNA concentration in the range from 0.3 to 15 μM, which indicates the absence of dimeric or higher order RNA complexes. Both AP34 and AP35 are less stable than the wild-type TAR hairpin, as reflected in a decrease of the melting temperatures. The difference of melting temperature T_m between the wild-type TAR and AP35 is small (0.6 °C), but the ΔG^0_{37} of AP35 is ~0.81 kcal/mol higher than that of the wild-type RNA. Thermodynamic parameters of AP34 are more evidently different. The T_m of AP34 is 3.2 °C lower and ΔG^0_{37} is 1.0 kcal/mol higher than that of wild-type TAR. Thus, the replacement of G^{34} by a AP leads to a significant destabilization of TAR hairpin that is more severe than the same substitution at position 35. These results indicate that residue G^{34} is more important

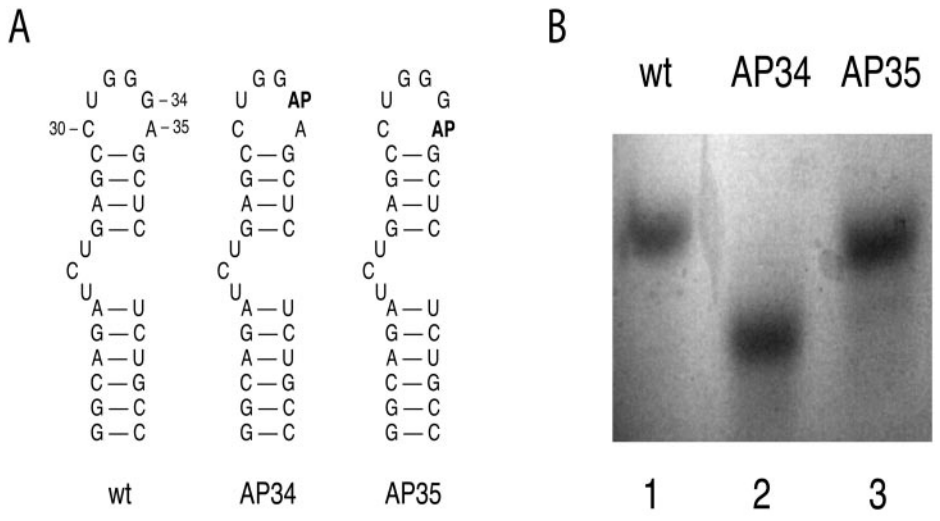

FIG. 2. **Non-denaturing gel electrophoresis of 29-mer TAR RNA with the wild-type sequence or 2-aminopurine substitutions at positions 34 or 35.** *A*, secondary structures of the wild-type, AP34, and AP35 hairpins. 2-aminopurine substitutions are indicated by AP. *B*, non-denaturing gel demonstrating differential mobility of the AP34 hairpin (*lane 2*) compared with the wild-type (*lane 1*) and AP35 hairpins (*lane 3*).

TABLE I
Thermodynamic parameters for the wild-type, AP34, and AP35 TAR hairpins

Values are averages of four independent experiments and were obtained by fitting experimental curves to a two-state model with sloping baselines through the use of a nonlinear least squares program MeltWin.

TAR RNA	ΔG^0_{37}	ΔH	ΔS	T_m	$\Delta\Delta G^0_{37}$	$\Delta\Delta H$	$\Delta\Delta S$
	kcal/mol	*kcal/mol*	*cal/K mol*	*°C*	*kcal/mol*	*kcal/mol*	*cal/K mol*
wt	−8.06 ± 0.09	−70.7 ± 2.1	−201.8 ± 4.0	76.5 ± 0.3			
ΔP34	−7.05 ± 0.11	−67.2 ± 1.9	−194.0 ± 5.1	73.3 ± 0.3	11.01	+3.5	+7.8
ΔP35	−7.25 ± 0.13	−65.1 ± 1.5	−186.5 ± 4.6	75.9 ± 0.4	+0.81	+5.6	+15.3

than A^{35} in maintaining a structured apical loop.

Lead-induced Cleavage of 2-Aminopurine-substituted TAR Hairpins—Metal ion promoted RNA cleavage can be used to map single stranded regions and metal coordination sites in an RNA structure (54). We previously used this approach to demonstrate that the TAR bulge binds metal ions in solution (33). Here, we used Pb^{2+}-induced cleavage to probe for changes in the TAR loop imposed by the 2-aminopurine substitutions. Overall, the cleavage pattern in the loop is quite similar for the wild-type and AP35 hairpins (Fig. 3). At the 5′-side of the loop, reactivity of the phosphodiester bond between C^{30}–U^{31} and U^{31}–G^{32} dominates the cleavage pattern. Cleavage is weaker at position C^{29}, reflecting less conformational freedom of this base paired residue. Toward the 3′-side of the loop, there are weak cleavages at G^{32}, G^{33}, and G^{34}, but backbone scission is more pronounced at residue G^{34}. The 2-aminopurine substitution in the AP34 hairpin strongly enhances the cleavage at position 34. Indeed, residue 34 is most prone to cleavage in the loop of the AP34 hairpin. This result indicates that the AP^{34} substitution results in an increased conformational flexibility of the TAR loop. In contrast, the intensity of cleavage at position 35 in AP35 is moderately decreased, indicating that the integrity of the apical loop is less sensitive to modification of residue 35. These results confirm that the loop structure is highly dependent on the nature of residue 34.

Molecular Dynamics Simulations of the TAR Apical Loop Structure—To evaluate the structural trends within the apical loop we have undertaken molecular dynamics (MD) simulations. We used two different approaches in preparing the initial model for MD simulations, thereby extending the conformational space searched for possible loop structures. In the first approach we have selected 1 out of 20 available NMR structures of the TAR RNA (34). We modeled the AP^{34} and AP^{35} substitutions onto the TAR structure to evaluate their effect on the loop conformation. In the second approach, we built models of a 14-mer TAR mini-hairpin (position 26–39) in which we imposed base pairing between C^{30} and G^{34}, followed by running the MD simulation without any constraints to investigate the stability of a C^{30}–G^{34} base pair.

The 29-mer wild-type TAR, AP34, and AP35 hairpins were built based on the coordinates of model No. 17 in PDB file 1ANR (30). The *in aqua* MD simulation for the wild-type hairpin was conducted for 1.6, and 1.0 ns simulations were performed for the AP34 and AP35 hairpins at 300 K. These simulations revealed considerable dynamics of the bulge and apical loop in all three hairpins. The C3′-*endo* sugar puckering was maintained largely in the residues of the double stranded stem. In the apical loop, sugar rings were considerably unstable. Frequent switches to the C2′-*endo* pucker and subsequent stabilization of this conformation was observed. Interestingly, loop residue 34 uniquely shows a stable C3′-*endo* pucker for all three hairpins. In all three cases, residue 35 retains its looped-out orientation. In the wild-type and AP35 simulations, residue 34 has a tendency to interact with the upper part of the double stranded region by stacking on the stem closing C^{29}–G^{36} base pair, but this stacking is much less pronounced for the AP34 hairpin (Fig. 4*A*). This may explain the contribution of residue 34 to the hairpin stability. Only few of the potential hydrogen-bonding contacts within the loop are stably observed, and these mainly involve residue G^{34} in the wild-type and AP35 hairpins. G^{34} can form a relatively stable hydrogen bond involving its O(6) and the $N(4)H_2$ of C^{30}. In parallel, the exo-NH_2 group of G^{34} interacts with the sugar moiety of C^{30}. In the AP35 hairpin, transient stacking interactions of C^{30} with U^{31}, and G^{32} with G^{33}, were observed despite considerable flexibility. In the final stages of the simulation with the AP34 hairpin, the 2-aminopurine at position 34 starts to interact more strongly with the looped out residue A^{35}. In general terms, the AP34 hairpin

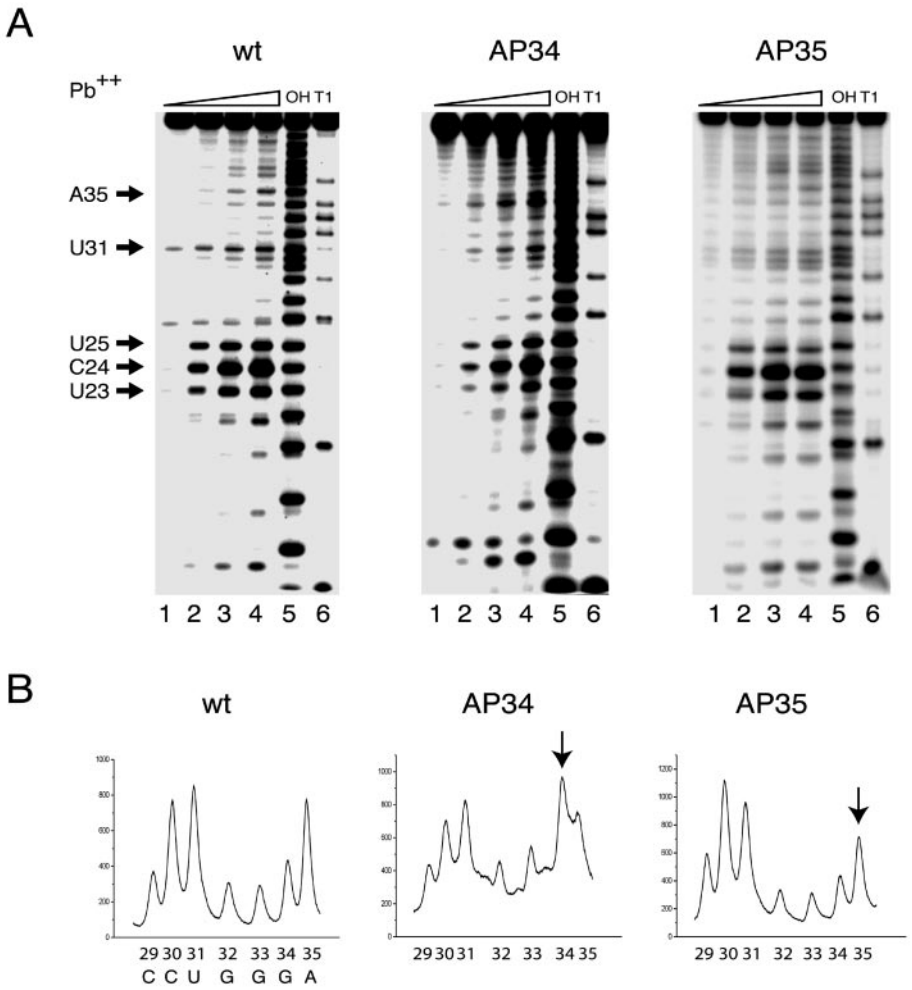

FIG. 3. **Lead-induced cleavage of the wild-type, AP34, and AP35 RNA.** *A*, autoradiograms of Lead-cleavage reactions performed at 0 (*lane 1*), 0.5 (*lane 2*), 1.0 (*lane 3*), and 2.0 mM (*lane 4*) $Pb(OAc)_2$. Partial hydrolosis (OH, *lane 5*) and RNase T1 sequencing reactions (T1, *lane 6*) were included for the identification of bands. Bands corresponding to positions U^{23}, C^{24}, U^{25}, and A^{35} are indicated by *arrows*. *B*, phosphorimager traces through *lane 2* (0.5 mM Pb^{2+}) of the gels shown in *A*, highlighting cleavages in the loop region of the wild-type, AP34, and AP35 RNA.

shows the least tendency toward a structured loop conformation during the simulation, which is consistent with the results from our experimental analyses.

To further investigate the possible interactions between C^{30} and G^{34}, we modeled the C^{30}–G^{34} base pair in a 14-mer TAR hairpin and then performed extensive MD simulations at different temperatures (Fig. 4, *B* and *C*). The initial models were built based by fitting the TAR sequence on the NMR structure of the HIV-1 A-rich hexaloop (PDB code 1bvj) (48). We selected this structure as a template for our modeling because of its well defined structural motif characterized by 3′-stacking of four adenosines in this hexaloop. The resulting structure was remodeled by imposing constraints for the C^{30}–G^{34} interaction, followed by running a short MD. This provided a set of initial structures for further MD investigations. All constraints were then removed and full MD trajectories were collected running simulations for 2 up to 8 ns, depending on the convergence of the simulated structures, at three different temperatures: 300, 320, and 340 K. This yielded a range of conformational motifs characterized by different internal interactions and exhibiting diverse stability and convergence within the MD trajectories in a total of 36 ns of simulation time.

The most stable MD trajectories were obtained with models that maintain the interaction between C^{30} and G^{34} (Fig. 4*C*). We consistently observed that C^{30} is repositioned slightly by stacking on the upper stem toward the major groove, exposing its Watson-Crick face across the loop toward G^{34}. Due to the local reorientation of the backbone around G^{34}, this base is shifted with respect to A^{35} and points across the loop toward C^{30}. In this orientation, all three Watson-Crick C–G hydrogen bonds across the loop were observed with high occupancy. As a consequence of the interaction between C^{30} and G^{34}, two sharp turns in the phosphodiester backbone are observed: the first between U^{31} and G^{32} and the second between G^{33} and G^{34}. We observed a strong tendency toward stacking interactions between G^{32} and G^{33}. This two-base stack is frequently oriented toward the outside of the loop, forming a structural module of relatively high mobility, although there are numerous events that disrupt this stacking in a reversible manner. These results indicate that hydrogen bonds between C^{30} and G^{34} are highly favorable and play a pivotal role in forming a structured conformation of the apical TAR loop. Additional interactions may stabilize this base pair. In particular, we observed additional hydrogen bonds between C^{30} and A^{35} in conjunction with the C^{30}–G^{34} base pair.

Site-directed Mutagenesis and Structure Probing of the C^{30}–G^{34} Base Pair—Because the previous analyses suggest the formation of a base pair between residues C^{30} and G^{34} within the TAR loop, we decided to directly test this possibility by generating mutant TAR constructs in which this base pair is either disrupted or replaced by another base pair. Six different mutants were made, comprising two sets in which the base pair is either disrupted or restored (Fig. 5*A*). Mutants G30 and C34 disrupt the proposed cross-loop base pair, which is potentially restored in the double mutant G30C34. Likewise, mutants U30 and A34 disrupt cross-loop pairing, but the double mutant U30A34 could form an alternative base pair.

We performed RNA structure probing on the wild-type and mutant TAR hairpins as 1–80 transcripts to evaluate the structural effects of these mutations in the loop. For the wild-type,

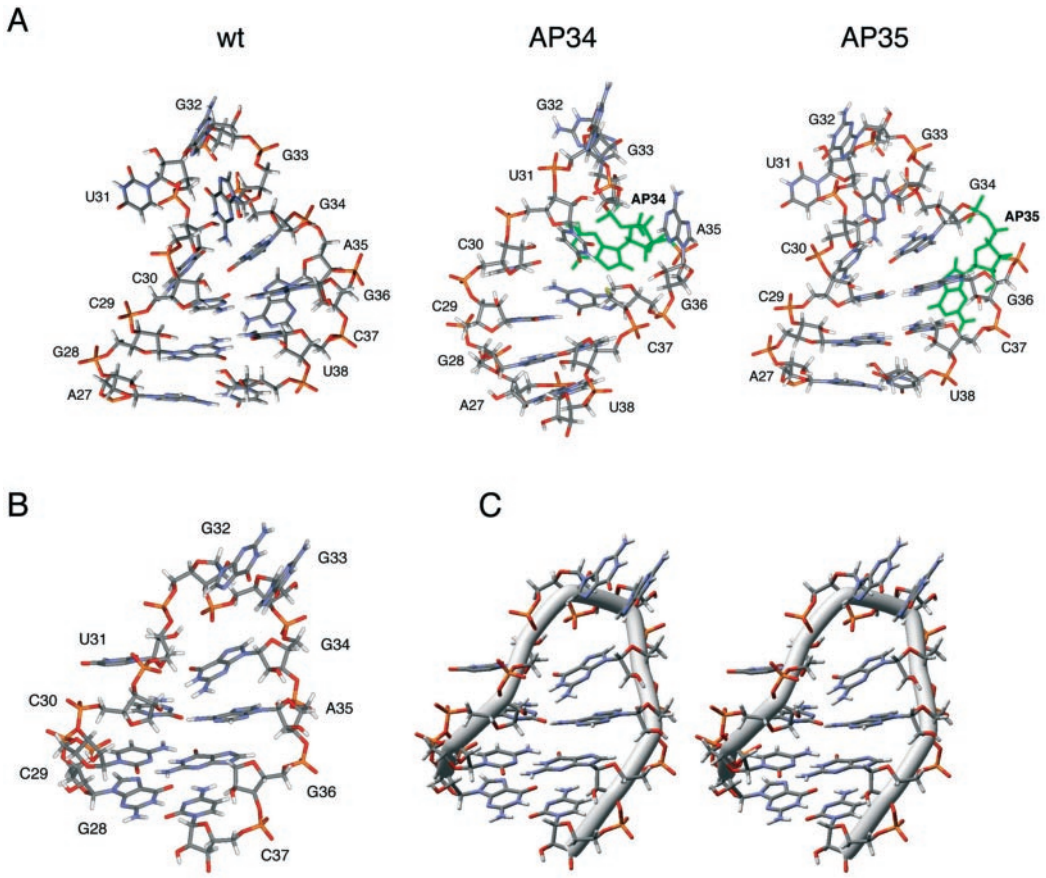

FIG. 4. **Molecular dynamics simulations of the TAR hairpin.** *A*, apical loop structures for the wt, AP34 and AP35 29-mer RNA hairpins (AP residue in *green*). *B*, structure of the wild-type TAR apical loop derived by molecular modeling and subsequent molecular dynamics simulations for the 14-mer RNA hairpin model. *C*, stereo image of the model shown in *B*.

our data are in good agreement with the secondary structure model of TAR. The single nucleotide bulges C^5 and A^{17} are both identified by DMS modification, as are U^{24} and U^{25} in the three-nucleotide bulge (Fig. 5*A*, *lane 3*). In addition, we observed DMS reactivity at A^{22}, which forms a distorted base pair with U^{40} just below the bulge and its sensitivity to DMS and DEPC has been documented repeatedly (10, 55). These features are maintained in all the mutant TAR elements, demonstrating that the loop mutations do not result in gross rearrangement of the TAR secondary structure. Structure probing of the wild-type TAR loop shows some characteristics of a structured loop. The three guanine residues are differentially modified by kethoxal, with reactivity being high at G^{32}, intermediate at G^{33} and low at G^{34} (Figs. 5*A*, *lane 2* and 6*B*, *wt*). The same pattern is observed when the RNA is probed with RNase T1 (results not shown) (11, 13, 37), and this observation was previously used to propose that G^{34} pairs with C^{30} (41). Indeed, C^{30} is protected from modification by DMS (Fig. 5*A*, *lane 3* and *C*, *wt*). U^{31} and A^{35} are sensitive to DMS modification, which confirms the exposure of the functional groups of these residues to the solvent.

Among the set of TAR loop mutants, significant changes in the probing profile are observed. The most severe effect is observed for mutants that have a base change at position 30 (G30, G30C34, U30, and U30A34), which results in the loss of the characteristic reactivity of the guanine residues (Fig. 5*A*, *lanes 8*, *11*, *17*, and *20*). G^{32} and G^{33} are no longer differentially modified and G^{34} is more reactive than in the wild-type context (Fig. 5*B*). Furthermore, the pattern of reverse transcriptase stops is redistributed by a loss of the stop at position 31 and the emergence of a novel stop at position 38 for all mutations at position 30 (Fig. 5*A*). These results indicate that C^{30} is instrumental in maintaining a structured TAR loop.

Mutation of position 34 has a less severe effect on the overall reactivities in the TAR loop, but it is apparent that both mutants C34 and A34 are reactive at position 34, whereas the wild-type G^{34} is not reactive (Fig. 5*A*, *lanes 6* and *15*, and Fig. 6*C*). In addition, both mutants exhibit increased reactivity of A^{35}, which indicates that mutation of residue 34 disturbs the local loop structure. For mutant A34, there is an additional increase in the reactivity of C^{30}, which is protected in the wild-type and in mutant C34 (Fig. 5*C*, mutant *A34*). Thus, substitution of G^{34} with an A results in exposure of residue C^{30}, presumably by displacing C^{30} from its stacked orientation on base pair C^{29}–G^{36}. The absence of increased reactivity at C^{30} in mutant C34 could be due to the presence of a pyrimidine at position 34 in this mutant, which may be insufficiently large to displace C^{30}.

Structure probing with the single mutants G30, U30, C33, and A34 demonstrates that the loop is significantly altered by these sequence changes and these results are compatible with the disruption of a base pair involving residues C^{30} and G^{34}. The double mutants G30C34 and U30A34 can form an alternative cross-loop base pair that may restore the loop structure. Close inspection of the base reactivities at positions 34 and 35 provides evidence that this may indeed be the case. We already showed that substituting G^{34} with C or A results in a high reactivity of the mutant residue 34 and an increase in reactivity of A^{35} (Fig. 5, *D* and *E*, respectively). Furthermore, substituting residue C^{30} with G or U reduces the reactivity of A^{35} (Fig. 5, *D* and *E*). In the double mutants G30C34 and U30A34, the reactivity of residue A^{35} is restored to levels similar to that

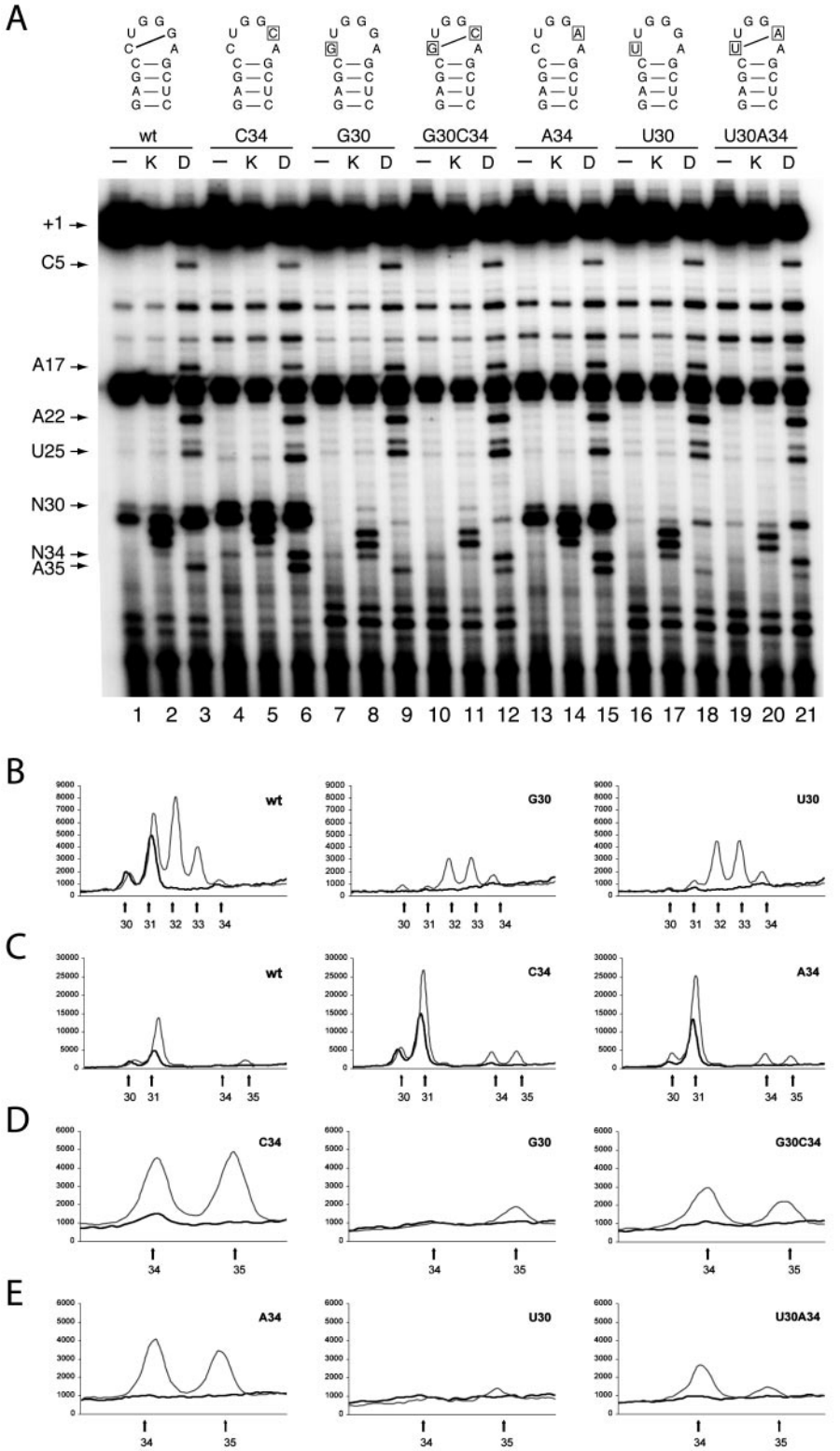

FIG. 5. **Chemical structure probing of wild-type and mutant HIV-1 RNA.** Secondary structures for the apical loop are shown at the *top*, mutant residues are *boxed*. *A*, gel showing the primer extension reactions on the untreated RNA (−: *lanes 1*, *4*, *7*, *10*, *13*, *16*, and *19*), kethoxal-treated (K: *2*, *5*, *8*, *11*, *14*, *17*, and *20*), and DMS-treated (D: *3*, *6*, *9*, *12*, *15*, *18*, and *21*). *Arrows* on the *left* mark positions where DMS reactivity was observed. *B*, *C*, *D*, and *E*, phosphorimager traces highlighting the loop residues were kethoxal (*B*) and DMS (*C*, *D*, and *E*) reactivities were observed. Chemically treated reactions are shown as *thin gray lines*, and *thick black lines* represent the untreated control. The identity of the RNA (wild-type or mutant) is indicated in the *upper right corner* of each graph. *Arrows* indicate the nucleotide positions.

of the wild-type TAR. In addition, residue 34 is slightly protected in the double mutants compared with the single mutants. Thus, the double mutants restore the wild-type behavior of residue A^{35} and possibly the base paring between residues 30 and 34.

Transcriptional Activity of LTR Promoters with a Wild-type or Mutant TAR Loop—We next assessed the effect of mutations in the TAR loop on the activity of the LTR promoter. C33A cells were transiently transfected with the wild-type and mutant LTR-luciferase reporter plasmids with and without a Tat expression plasmid. In the absence of Tat, the wild-type and mutant TAR elements have similar LTR activity, indicating that basal transcription is not influenced by the structure of the TAR loop (Fig. 6*A*). The wild-type LTR activity with Tat was set at 100%, corresponding to a 24-fold activation over the basal activity without Tat (Fig. 6, *A* and *B*). Mutants C34 and A34 cause the most severe reduction in Tat-mediated transcriptional activation, with a modest 2-fold LTR activation. Mutants G30 and U30 have a less severe effect, but the Tat response is significantly reduced to 6-fold. The double mutant

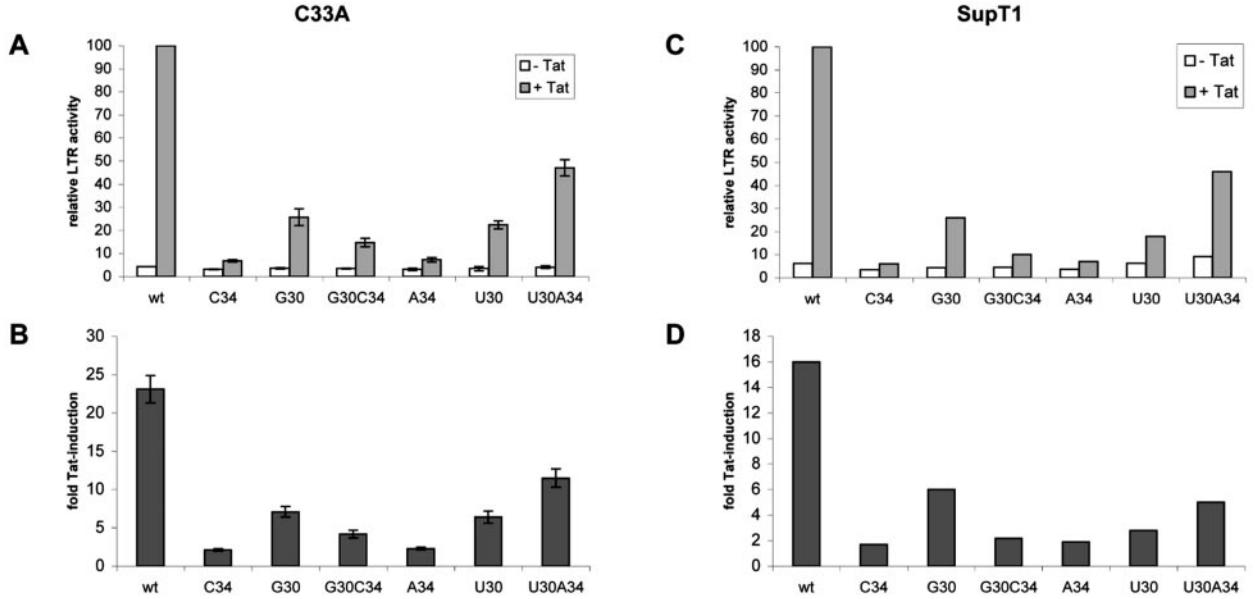

FIG. 6. **LTR-luciferase assays with wild-type and mutant constructs.** *A*, LTR activity measured in C33A cells in the absence and presence of a Tat-expressing vector. *B*, fold promoter induction as measured in C33A cells. *C*, LTR activity measured in SupT1 cells in the absence and presence of a Tat-expressing vector. *D*, fold promoter induction as measured in SupT1 cells.

G30C34 reaches a Tat response of about 5-fold, a phenotype that is intermediate between that of the two individual mutants G30 and C34. Thus, the double mutant partially compensates for the defect caused by the C^{34} mutation. This compensatory effect is more prominent for the double mutant U30A34, which demonstrates a Tat response that exceeds the level observed for the individual mutants U30 and A34. These results indicate that the base pair between residues 30 and 34 plays a role in Tat-mediated activation of the LTR promoter, but has no effect on basal transcription. Similar results were obtained in the SupT1 T-cell line (Fig. 6, *C* and *D*), indicating that these effects hold true in the cell type that is physiologically relevant to HIV-1 infection.

DISCUSSION

The structure of the HIV-1 TAR element has been studied extensively, but the conformation of the apical loop has remained elusive. Based on structure probing and modeling, it has been suggested that the TAR loop is structured through a cross-loop base pair involving nucleotides C^{30} and G^{34} (41), but this model has received little attention. Recently, hydrogen bonds involving G^{34} have been implied in stabilizing the apical loop (34) and the C^{30}–G^{34} base pair was observed transiently in molecular dynamics simulations (56). Furthermore, binding of cyclin T1 to TAR appears to require this base pair (42). To date, it has not been demonstrated whether a structured conformation of the TAR loop is required for trans-activation of the LTR promoter.

The results we present in this study further support the notion that the TAR loop is stabilized by the C^{30}–G^{34} cross-loop base pair. We observed destabilization of the TAR hairpin upon mutation of the loop, indicating that the wild-type sequence contributes to the overall stability of the TAR hairpin. Studies with model TAR hairpins containing 2-aminopurine riboside substitutions in the loop support this idea. Non-denaturing PAGE analysis and lead-probing showed that G^{34} plays a key role in maintaining a structured TAR loop. Introducing the modified base at position 34 (AP34) alters two putative Watson-Crick hydrogen bonds because the acceptor-donor properties of the functional groups at the position 1 and 6 of the guanosine are changed. The corresponding change in free energy that was measured for AP34 is within the range associated with the elimination of one or two hydrogen bonds (57).

The molecular modeling and MD simulations demonstrate that the TAR loop has a tendency to adopt a stable structure through internal hydrogen bonds. We observed a base-specific interaction between C^{30} and G^{34} involving the O(6) of G^{34} and the $N(4)H_2$ of C^{30} in MD simulations of the 29-mer TAR RNA. Further MD simulations on the 14-mer TAR model hairpin indicated that all Watson-Crick hydrogen bonds between C^{30} and G^{34} can be formed. The geometry of these interactions may be distorted, which could explain why the base pair was not readily detected in previous NMR studies. Close inspection of these NMR-derived structure models provides further evidence that hydrogen bonds between residues C^{30} and G^{34} are possible within the TAR apical loop. These TAR models show a strong tendency for an in-loop orientation of G^{34} by stacking on G^{36}, and this exposes the Watson-Crick side toward C^{30} (30). Indeed, this is consistent with a NOE sequential contact between H8-G^{34} and H8-G^{36} (30). C^{30} efficiently stacks on C^{29}, but commonly adopts an orientation away from G^{34}. However, several structure models in the ensemble allow for hydrogen bonding between C^{30} and G^{34}. Previously, it has proven difficult to assign the imino proton resonances of G^{32}, G^{33}, and G^{34} in NMR studies of the HIV-1 TAR hairpin. In one study these remained unassigned (11.05, 10.86, and 10.62 ppm) (39), while in another the assignment was nonspecific (11.58 (G^{32}), 10.82 (G^{33}), and 10.59 (G^{34}) ppm) (29). Two of these resonances are within the range of unpaired guanines, but one consistently appears off range above 11.00 ppm. The participation of G^{34} in a pairing interaction with C^{30} would be consistent with assigning the off-range resonance to G^{34}.

RNA structure probing of the wild-type TAR RNA and mutants with a disrupted or substituted base pair at positions 30 and 34 showed base reactivity changes that are consistent with the presence of a C^{30}–G^{34} base pair. Reactivity changes at positions 34 and 35 in the double mutants compared with single mutants indicated that the double mutants may partially restore an interaction between residues 30 and 34. In LTR-luciferase assays, we observed a partial rescue of the Tat response with the G30C34 double mutant and true rescue with

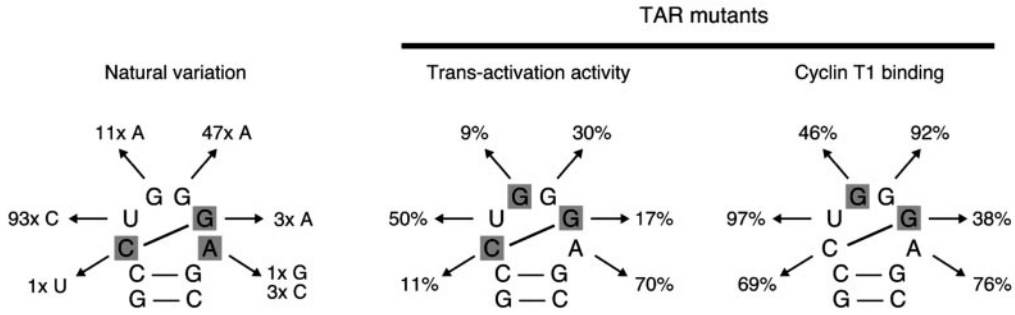

FIG. 7. **Phylogenetic analysis and summary of previous mutagenesis studies of the HIV TAR loop.** The phylogenetic survey is based on 654 complete TAR sequences from the HIV-1 sequence data base. Trans-activation data are from Refs. 68 and 5. Cyclin T binding data are from Ref. 42. In case of the mutational analyses, the wild-type activity was set at 100%, and *arrows* indicate the relative activity measured after mutation of the corresponding nucleotide.

the U30A34 double mutant as compared with constructs with the individual mutations. This demonstrates that the cross-loop base pair is required for Tat-mediated trans-activation of the HIV-1 promoter. The mutant analysis also suggests that this requires a 5′-pyrimidine and a 3′-purine in the cross-loop base pair, since mutant G30C34 only partially rescues transcriptional activation. Because the U30A34 mutant does not reach wild-type levels of promoter activity in the presence of Tat, it is likely that the sequence as well as the structure of the TAR loop contribute to the optimal Tat response of the LTR promoter.

Recently, two groups have independently recognized the frequent occurrence of RNA loops containing a cross-loop base pair capped by a tri-loop in ribosomal RNA, and each proposed a different nomenclature for this motif, the T-loop or the lone pair triloop (58, 59). There are several additional examples of analogous six-nucleotide RNA loops in which the first and fifth residue form a cross-loop base pair. This loop structure has been identified in the TΨC loop of the yeast phenylalanine tRNA ((60) and references therein), the anticodon loop of the yeast aspargine tRNA (61), the Iron Responsive Element (62, 63), the subgenomic promoter of the brome mosaic virus (64), the encapsidation signal of the Hepatitis B virus (65) and the internal ribosomal entry site of the hepatitis C virus (66, 67). The vast majority of these loops constitute important protein binding sites, and in each case the first loop nucleotide is a pyrimidine and the fifth is a purine. This loop architecture appears to be strongly conserved, despite considerable sequence variation and differences in the hydrogen bonding of the cross-loop base pair; deviations from canonical Watson-Crick pairing across the loop are common (59). Our results demonstrate that the apical loop of the HIV-1 TAR hairpin fits the description of this T-loop or lone pair triloop motif.

In this study, we used a limited number of mutants to investigate the structure of the TAR loop: a triple mutant in which ^{32}GGG^{34} is changed to AAA, two hairpins containing 2-aminopurine substitutions at positions 34 and 35, and a set of six mutants with point mutations at positions 30 and 34. Thus, the contribution of mutations at positions 31, 32, and 33 was not tested. However, comprehensive mutational analyses of the apical loop have previously been performed (5, 42, 68), and we summarized these results in Fig. 7. In addition, we performed a comparative sequence analysis of natural HIV-1 isolates that highlights the sequence variation within the loop. Residues 30, 34 and 35 are strongly conserved, with substitutions in only 1 (C^{30}), 3 (G^{34}), and 4 (A^{35}) out of 654 sequences. In transactivation assays, mutations at residues C^{30}, G^{32}, and G^{34} have the most dramatic effect on the Tat response of the LTR promoter (5, 68). Binding of cyclin T1 is most sensitive to mutations at positions G^{32} and G^{34}, and a small contribution of C^{30} to cyclin T1 binding was observed (42). Interestingly, the same study demonstrated that the loss of protein binding due to mutation of residue 34 is partially rescued by a complementary sequence change at position 30. Throughout these different analyses, C^{30} and G^{34} consistently emerge as conserved and functionally important residues, which is compatible with the structured conformation of the TAR loop containing a C^{30}–G^{34} cross-loop base pair.

We observed that the structure of the TAR apical loop affects the Tat-dependent phase of transcription from the LTR promoter and this suggests that the structured loop conformation may be involved in the interaction between TAR and cyclin T1. Indeed, our results complement the study of Richter *et al.* (42), which demonstrated that binding of cyclin T1 to TAR is most efficient when the cross-loop base pair can form. However, the extent to which our mutant U30A34 rescues Tat-dependent promoter activity significantly exceeds the rescue of cyclin T1 binding by the analogous mutant in Richter's study. This suggests that the role of the TAR loop in Tat-dependent transcription may not be exclusively attributable to the TAR-cyclin T1 interaction. Indeed, cyclin T1 also affects transcription at the LTR promoter independently of its interaction with TAR (69). In addition, other cellular proteins that bind to the TAR loop have been described (20, 70–72) and may require the C^{30}–G^{34} cross-loop base pair for recognition of TAR.

Acknowledgments—We thank Wim van Est for preparing the figures and René Olsthoorn and Joost Haasnoot for fruitful discussions. Access to CRAY J916 at the Poznañ Supercomputing and Networking Centre is acknowledged.

REFERENCES

1. Hamy, F., Felder, E. R., Heizmann, G., Lazdins, J., Aboul-ela, F., Varani, G., Karn, J., and Klimkait, T. (1997) *Proc. Natl. Acad. Sci. U. S. A.* **94,** 3548–3553
2. Jones, K. A., Kadonaga, J. T., Luciw, P. A., and Tjian, R. (1986) *Science* **232,** 755–759
3. Harrich, D., Garcia, J., Wu, F., Mitsuyasu, R., Gonzalez, J., and Gaynor, R. (1989) *J. Virol.* **63,** 2585–2591
4. Berkhout, B., and Jeang, K. T. (1992) *J. Virol.* **66,** 139–149
5. Berkhout, B., and Jeang, K. T. (1989) *J. Virol.* **63,** 5501–5504
6. Frankel, A. D., Biancalana, S., and Hudson, D. (1989) *Proc. Natl. Acad. Sci. U. S. A.* **86,** 7397–7401
7. Roy, S., Parkin, N. T., Rosen, C., Itovitch, J., and Sonenberg, N. (1990) *J. Virol.* **64,** 1402–1406
8. Dingwall, C., Ernberg, I., Gait, M. J., Green, S. M., Heaphy, S., Karn, J., Lowe, A. D., Singh, M., and Skinner, M. A. (1990) *EMBO J.* **9,** 4145–4153
9. Sumner-Smith, M., Roy, S., Barnett, R., Reid, L. S., Kuperman, R., Delling, U., and Sonenberg, N. (1991) *J. Virol.* **65,** 5196–5202
10. Weeks, K. M., and Crothers, D. M. (1991) *Cell* **66,** 577–588
11. Harper, J. W., and Logsdon, N. J. (1991) *Biochemistry* **30,** 8060–8066
12. Muesing, M. A., Smith, D. H., and Capon, D. J. (1987) *Cell* **48,** 691–701
13. Wei, P., Garber, M. E., Fang, S.-M., Fisher, W. H., and Jones, K. A. (1998) *Cell* **92,** 451–462
14. Zhang, J., Tamilarasu, N., Hwang, S., Garber, M. E., Huq, I., Jones, K. A., and Rana, T. M. (2000) *J. Biol. Chem.* **275,** 34314–34319
15. Berkhout, B., Silverman, R. H., and Jeang, K. T. (1989) *Cell* **59,** 273–282
16. Dorin, D., Bonnet, M. C., Bannwarth, S., Gatignol, A., Meurs, E. F., and Vaquero, C. (2003) *J. Biol. Chem.* **278,** 4440–4448
17. Chepenik, L. G., Tretiakova, A. P., Krachmarov, C. P., Johnson, E. M., and Khalili, K. (1998) *Gene* (*Amst.*) **210,** 37–44

18. Han, X. M., Laras, A., Rounseville, M. P., Kumar, A., and Shank, P. R. (1992) *J. Virol.* **66,** 4065–4072
19. Wu-Baer, F., Sigman, D., and Gaynor, R. B. (1995) *Proc. Natl. Acad. Sci. U. S. A.* **92,** 7153–7157
20. Wu, F., Garcia, J., Sigman, D., and Gaynor, R. (1991) *Genes Dev.* **5,** 2128–2140
21. Gatignol, A., Buckler-White, A., Berkhout, B., and Jeang, K. T. (1991) *Science* **251,** 1597–1600
22. Wimmer, J., Fujinaga, K., Taube, R., Cujec, T. P., Zhu, Y., Peng, J., Price, D. H., and Peterlin, B. M. (1999) *Virology.* **255,** 182–189
23. Richter, S., Ping, Y. H., and Rana, T. M. (2002) *Proc. Natl. Acad. Sci. U. S. A.* **99,** 7928–7933
24. Bieniasz, P. D., Grdina, T. A., Bogerd, H. P., and Cullen, B. R. (1999) *Proc. Natl. Acad. Sci. U. S. A.* **96,** 7791–7796
25. Parada, C. A., and Roeder, R. G. (1996) *Nature* **384,** 375–378
26. Marciniak, R. A., and Sharp, P. A. (1991) *EMBO J.* **10,** 4189–4196
27. Puglisi, J. D., Tan, R., Calnan, B. J., Frankel, A. D., and Williamson, J. R. (1992) *Science* **257,** 76–80
28. Aboul-ela, F., Karn, J., and Varani, G. (1996) *Nucleic Acids Res.* **24,** 3974–3981
29. Long, K. S., and Crothers, D. M. (1999) *Biochemistry* **38,** 10059–10069
30. Aboul-ela, F., Karn, J., and Varani, G. (1995) *J. Mol. Biol.* **253,** 313–332
31. Faber, C., Sticht, H., Schweimer, K., and Rosch, P. (2000) *J. Biol. Chem.* **275,** 20660–20666
32. Ippolito, J. A., and Steitz, T. A. (1998) *Proc. Natl. Acad. Sci. U. S. A.* **95,** 9819–9824
33. Olejniczak, M., Gdaniec, Z., Fischer, A., Grabarkiewicz, T., Bielecki, L., and Adamiak, R. W. (2002) *Nucleic Acids Res.* **30,** 4241–4249
34. Kulinski, T., Bielecki, L., Olejniczak, M., Zagórowska, I., and Adamiak, R. W. (1999) *Collect. Czech. Chem. Commun. Symp. Ser.* **2,** 191–196
35. Nifosi, R., Reyes, C. M., and Kollman, P. A. (2000) *Nucleic Acids Res.* **28,** 4944–4955
36. Leulliot, N., and Varani, G. (2001) *Biochemistry* **40,** 7947–7956
37. Colvin, R. A., and Garcia-Blanco, M. A. (1992) *J. Virol.* **66,** 930–935
38. Michnicka, M. J., Harper, J. W., and King, G. C. (1993) *Biochemistry* **32,** 395–400
39. Jaeger, J. A., and Tinoco, I., Jr. (1993) *Biochemistry* **32,** 12522–12530
40. King, G. C., Harper, J. W., and Xi, Z. (1995) *Methods Enzymol.* **261,** 436–450
41. Critchley, A. D., Haneef, I., Cousens, D. J., and Stockley, P. G. (1993) *J. Mol. Graph.* **11,** 92–97
42. Richter, S., Cao, H., and Rana, T. M. (2002) *Biochemistry* **41,** 6391–6397
43. Usman, N., Ogilvie, K. K., Jiang, M. Y., and Cedergren, R. J. (1987) *J. Am. Chem. Soc.* **109,** 7845–7854
44. Pearlman, D. A., Case, D. A., Caldwell, J. W., Ross, W. S., Cheatham, T. E., DeBolt, S., Ferguson, D., Seibel, G., and Kollman, P. (1995) *Comput. Phys. Commun.* **74,** 1–41
45. Frisch M. J., Trucks G. W., Schlegel H. B., Gill P. M. W., Johnson B. G., Robb M. A., Cheeseman J. R., Raghavachari K., Al-Laham M. A., Zakrzewski V. G., Ortiz J. V., Foresman J. B., Cioslowski J., Stefanov B. B., Nanayakkara A., Challacombe M., Peng C. Y., Ayala P. Y., Chen W., Wong M. W., Andres J. L., Replogle E. S., Gomperts R., Martin R. L., Fox D. J., Binkley J. S., Defrees D. J., Baker J., Stewart J. J. P., Head-Gordon M., Gonzalez C., and Pople J. A. (1996) *Gaussian 94*, Gaussian, Inc., Pittsburgh, PA
46. Cieplak, P., Cornell, W. D., Bayly, C., and Kollman, P. A. (1995) *J. Comp. Chem.* **16,** 1357–1377
47. York, D. M., Darden, T. A., and Pedersen, L. G. (1993) *J. Chem. Phys.* **99,** 8345–8348
48. Puglisi, E. V., and Puglisi, J. D. (1998) *Nat. Med.* **5,** 1033–1036
49. Foloppe, N., and MacKerell, A. D. (2000) *J. Comp. Chem.* **21,** 86–104
50. Huthoff, H., and Berkhout, B. (2001) *RNA* **7,** 143–157
51. Jeeninga, R. E., Hoogenkamp, M., Armand-Ugon, M., de Baar, M., Verhoef, K., and Berkhout, B. (2000) *J. Virol.* **74,** 3740–3751
52. Verhoef, K., Koper, M., and Berkhout, B. (1997) *Virology* **237,** 228–236
53. Das, A. T., Klaver, B., and Berkhout, B. (1999) *J. Virol.* **73,** 81–91
54. Ciesiolka, J., Marciniec, T., and Krzyzosiak, W. (1989) *Eur. J. Biochem.* **182,** 445–450
55. Baudin, F., Marquet, R., Isel, C., Darlix, J. L., Ehresmann, B., and Ehresmann, C. (1993) *J. Mol. Biol.* **229,** 382–397
56. Reyes, C. M., Nifosi, R., Frankel, A. D., and Kollman, P. A. (2001) *Biophys. J.* **80,** 2833–2842
57. SantaLucia, J., Jr., Kierzek, R., and Turner, D. H. (1992) *Science* **256,** 217–219
58. Nagaswamy, U., and Fox, G. E. (2002) *RNA* **8,** 1112–1119
59. Lee, J. C., Cannone, J. J., and Gutell, R. R. (2003) *J. Mol. Biol.* **325,** 65–83
60. Shi, H., and Moore, P. B. (2000) *RNA* **6,** 1091–1105
61. Moras, D., Comarmond, M. B., Fischer, J., Weiss, R., Thierry, J. C., Ebel, J. P., and Giege, R. (1980) *Nature* **288,** 669–674
62. Laing, L. G., and Hall, K. B. (1996) *Biochemistry* **35,** 13586–13596
63. Gdaniec, Z., Sierzputowska-Gracz, H., and Theil, E. C. (1998) *Biochemistry* **37,** 1505–1512
64. Haasnoot, P. C., Brederode, F. T., Olsthoorn, R. C., and Bol, J. F. (2000) *RNA* **6,** 708–716
65. Flodell, S., Schleucher, J., Cromsigt, J., Ippel, H., Kidd-Ljunggren, K., and Wijmenga, S. (2002) *Nucleic Acids Res.* **30,** 4803–4811
66. Lukavsky, P. J., Otto, G. A., Lancaster, A. M., Sarnow, P., and Puglisi, J. D. (2000) *Nat. Struct. Biol* **7,** 1105–1110
67. Klinck, R., Westhof, E., Walker, S., Afshar, M., Collier, A., and Aboul-ela, F. (2000) *RNA* **6,** 1423–1431
68. Feng, S., and Holland, E. C. (1988) *Nature* **334,** 165–167
69. Yedavalli, V. S., Benkirane, M., and Jeang, K. T. (2003) *J. Biol. Chem.* **278,** 6404–6410
70. Sheline, C. T., Milocco, L. H., and Jones, K. A. (1991) *Genes Dev.* **5,** 2508–2520
71. Marciniak, R. A., Garcia Blanco, M. A., and Sharp, P. A. (1990) *Proc. Natl. Acad. Sci. U. S. A.* **87,** 3624–3628
72. Kaczmarski, W., and Khan, S. A. (1993) *Biochem. Biophys. Res. Commun.* **196,** 935–942